Available online at www.sciencedirect.com
SCIENCE DIRECT®

Journal of the European Ceramic Society 24 (2004) 3129–3138
www.elsevier.com/locate/jeurceramsoc

Crystallographical analysis of surface layers of refractory ceramics formed using combined flame spray and simultaneous laser treatment

J.F. Li[a,b,*], L. Li[b], F.H. Stott[a]

[a]*Corrosion and Protection Centre, University of Manchester Institute of Science and Technology (UMIST), PO Box 88, Manchester M60 1QD, UK*
[b]*Laser Processing Research Centre, Department of Mechanical, Aerospace and Manufacturing Engineering, UMIST, PO Box 88, Manchester M60 1QD, UK*

Received 24 July 2003; received in revised form 27 October 2003; accepted 1 November 2003

Abstract

The crystalline characteristics of the surface layers of an alumina-based refractory ceramic, prepared using a novel combined flame spraying and laser melting method, have been investigated using X-ray diffraction and the Rietveld method. The results have indicated that 20% Cr_2O_3 by weight added to Al_2O_3 powder retards the metastable γ-Al_2O_3 to α-Al_2O_3 phase transition during flame spraying. The mullite crystals grew preferentially along the [111] direction for surface layers prepared by laser melting only or by the combined process using pure Al_2O_3 powder as the feedstock for flame spraying. In the latter case, the surface layer contained more alumina-rich mullite and more crystalline cristobalite than the surface layer prepared by laser melting. However, using a composite powder of 20% Cr_2O_3 and 80% Al_2O_3 by weight as feedstock in the combined process, not only did the preferred orientation of the mullite grains change to the [220] direction, but, also, the amount of SiO_2 incorporated in the mullite crystals was closer to that for stoichiometric mullite.

Keywords: Flame spraying; Laser hybrid processing; Mullite; Refractories; X-ray methods

1. Introduction

A combined flame spraying and simultaneous CO_2 laser surface treatment method has been developed as an accelerated process relative to the laser surface melting method for improving the surface structural integrity of aluminosilicate refractories.[1–4] Moreover, by applying a higher grade of powder as the feedstock for the flame spraying part of the combined process, chemical surface modification of refractory ceramics could be achieved. Previous investigations of the process have indicated that both the laser irradiation intensity and the powder feed rate are critical factors for attaining treated surface layers, with relatively dense microstructures and containing fewer cracks.[1,2] These improvements are due to the predominant mullite phase in the resulting surface layer. An area coverage rate of 20 mm^2/s has been used to produce a treated surface layer, approximately 2 mm in thickness, with improved structural integrity and performance.[2]

Mullite is an important structural and refractory ceramic, having very good strength and creep properties. Extensive work has been carried out to characterize its composition and crystalline structure.[5,6–9] The mullite crystals used in much work were synthesized by liquid-phase sintering of alumina–silica systems in the temperature range: 1100–1600 °C. It is known that the composition and crystalline structure of mullite depend on the chemical constituents of the precursor and the formation temperature. Commonly, the chemical formula of mullite is written as[5]

$$Al_{4+2x}Si_{2-2x}O_{10-x} \quad (1)$$

* Corresponding author. Tel.: +44-161-200-3827; fax: +44-161-200-3803.
E-mail address: j.li-3@umist.ac.uk (J.F. Li).

0955-2219/$ - see front matter © 2003 Elsevier Ltd. All rights reserved.
doi:10.1016/j.jeurceramsoc.2003.11.002

The value of x varies from 0.17 to 0.59 and changes in x result in changes in the lattice constants. The crystalline structure of mullite is generally orthorhombic, while that of mullite with a high alumina content (large value of x) is sometimes referred to as being pseudotetragonal because the a-lattice and b-lattice parameters are approximately equal in length. Recently, laser melting has been used to synthesize structural mullite fibers.[10] The as-drawn fibers were amorphous and required subsequent heat treatment to crystallize them. Direct formation of mullite crystals in CO_2 laser treated surface layers of aluminosilicate ceramics was first noted by Lambert et al.,[11] and was also reported by Bradley et al.[3] These mullite crystals were produced by rapid solidification of laser-induced aluminosilicate melts, a different method of formation from liquid-phase sintering. However, the compositions and crystalline structures of the mullite crystals formed during such laser surface treatment have not been characterized in detail.

In the present work, surface layers on an alumina-based refractory ceramic were modified using the combined process of flame spraying and laser surface treatment, using various combinations of flame spraying and laser melting. Two types of powders, pure Al_2O_3 and 20 wt.%Cr_2O_3–80 wt.%Al_2O_3 composite powders, were used as the feedstocks for the flame spraying technique in the combined process. The aim was to identify the effects of the process conditions and powder type on the development of crystalline phases, in terms of phase content, preferred orientation and lattice parameters of the main phase, mullite, in the treated surface layers, by X-ray diffraction. The lattice parameters of the mullite crystals in the various surface layers were determined using the X-ray Rietveld method.

2. Experimental

2.1. Flame spray feedstocks and workpiece material

The pure Al_2O_3 was Sulzer-Metco 105SFP powder (Sulzer-Metco, Switzerland), which is a fused and crushed alumina powder, α-Al_2O_3 plus small amounts of β-Al_2O_3, of particle size $-25+5$ μm. The 20 wt.%Cr_2O_3–80 wt.%Al_2O_3 was a mechanically blended powder of 80% Sulzer-Metco 105SFP and 20% Cr_2O_3 by weight. The Cr_2O_3 was the FST C-604.22 powder (Flame Spray Technologies b. v., Netherlands), also a fused and crushed chromium oxide powder, eskolaite, of particle size $-45+10$ μm. A typical scanning electron microscopy (SEM) micrograph of the mechanically blended 20 wt.%Cr_2O_3–80 wt.%Al_2O_3 powder was presented in a previous paper,[1] showing that there were no significant morphological differences between the Cr_2O_3 and Al_2O_3 particles.

The workpiece was the same as that detailed in a previous paper.[1] It was a 60% alumina-based refractory ceramic provided by Cleanaway Ltd. in the form of bricks, approximately $200\times200\times100$ mm, typically used to line furnaces and incinerators. It contained 60.0% Al_2O_3, 35.0% SiO_2, 1.6% P_2O_5, 1.4% TiO_2, 0.9% Fe_3O_4, 0.3% MgO, 0.3% Na_2O, 0.2% K_2O and 0.2% CaO by weight, and was mainly mullite with about 5% cristobalite by weight. Fig. 1 presents X-ray diffraction (XRD) spectra for the two types of feedstock powders and the refractory brick. The XRD spectrum for the brick was collected from particles, less than 75 μm in diameter, following manual crushing and milling using an alumina mortar. Prior to surface treatment using the combined process, the as-received refractory bricks were

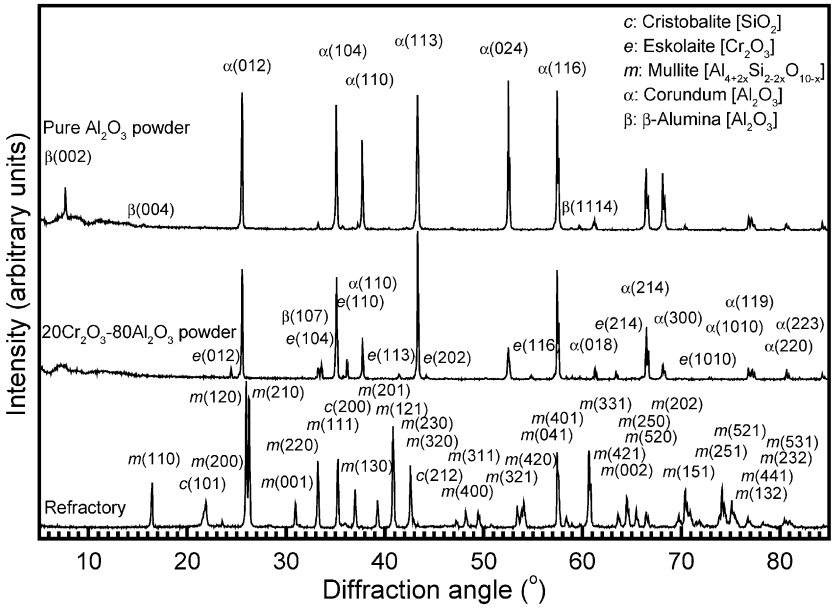

Fig. 1. XRD spectra for the feedstock powders and the refractory brick, identifying their phase constituents.

sectioned into squares, 80×50×20 mm. As can be seen from SEM images of cross sections of the treated surface layers presented in the next section, cracks and open surface pores, as well as mullite aggregates, 1–5 mm in size, are visible on the untreated regions.

2.2. The combined flame spraying and laser treating method

The combined process set up consisted of a Sulzer-Metco Type 6P-II thermospray gun and a Rofin-Sinar CO_2 laser (Rofin-Sinar, Germany) emitting at 10.6 μm and operating in the continuous wave (CW) TEM^*_{01} mode, with a maximum output power of 1.2 kW (Fig. 2). Feedstock powder particles for the flame spraying method were injected into the flame jet where they were partially melted and propelled towards the workpiece surface moving at a certain traverse velocity, to produce a coating. At the same time, a continuous CO_2 laser, of sufficient intensity, was incident on the produced coating, leading to the formation of a melt pool, due to a very intensive heat flux. The melt pool then solidified to produce a dense treated track. Treated surface layers of large area were accomplished by using successive treated tracks with an overlapping ratio of approximately 50%.

The sample codes of the samples and corresponding process conditions investigated are listed in Table 1. The process conditions for samples LFAA and LFCA, prepared using pure Al_2O_3 and 20 wt.%Cr_2O_3–80 wt.%Al_2O_3 powders as feedstocks, respectively, resulted in the treated surface layers having relatively few cracks. Sample L000 was prepared using laser surface melting only, while sample LF00 was prepared using the same process parameters as samples LFAA and LFCA, but without use of a powder feedstock for the flame spraying part of the process. For the above four samples, the laser beam was circular with a cross-sectional geometry, 16 mm in diameter. In addition, two flame sprayed samples, FAA and FCA, were also prepared for comparison. Except for the process parameters listed in Table 1, the other flame and laser process parameters were all the same as those reported in the previous paper,[1] and, hence, are not repeated here.

2.3. X-ray diffraction

The XRD data were obtained using a Philip X'pert APD, PW3710 diffractometer (Philips Co., Netherlands). Initial XRD spectra were collected from as-treated surfaces of the samples to identify the phase constituents and determine the crystalline orientations of the main phase, mullite. The experimental conditions included a Cu target, operating at 50 kV and 40 mA, a 0.5° automatic divergent slit and a 0.05 mm receiving slit. The collected data angles (2θ) ranged from 5.025 to 84.975° with a step size of 0.05° and a counting time of 2.0 s per step. Subsequently, the treated surface layers of samples L000, LF00, LFAA and LFCA were removed from the substrates using a Struers Accutom-5 cutting machine (Struers, Germany), and manually crushed and milled into particles less than 75 μm in diameter, using an alumina mortar. XRD spectra were collected from these milled particles and from particles of the as-received refractory ceramic, and the lattice parameters of the mullite crystals and the contents of crystalline phases were determined using the Rietveld method.[12] The aims were to characterize the crystalline structures of the mullite crystals formed by the combined flame

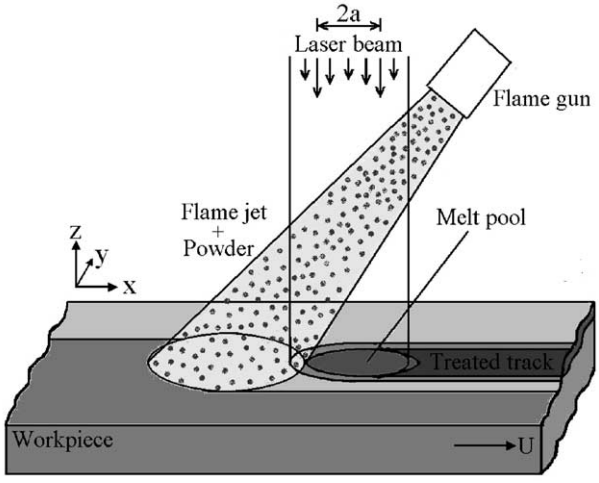

Fig. 2. Schematic diagram showing the combined process set up for the flame spraying and laser surface treatment process.

Table 1
Sample codes and corresponding process parameters

Sample code	Laser power (W)	Flame spraying (on/off)	Powder type	Powder feed rate (g/min)	Workpiece traverse velocity (mm/s)
FAA	0	On	Pure Al_2O_3	3.0	4
FCA	0	On	20%Cr_2O_3–80%Al_2O_3	3.2	4
L000	1000	Off	...	...	4
LF00	1000	On	...	...	4
LFAA	1000	On	Pure Al_2O_3	3.0	4
LFCA	1000	On	20%Cr_2O_3–80%Al_2O_3	3.2	4

spraying and laser melting process, and to ascertain the effects of the process conditions and powder type on the lattice parameters of the mullite crystals. The experimental conditions were a Cu target, operated at 50 kV and 40 mA, a 0.25° fixed divergent slit and a 0.20 mm receiving slit. The collected data angles (2θ) ranged from 5 to 120° with a step size of 0.04° and a counting time of 60 s per step.

The Rietveld analysis was carried out using the Rietica program for Windows, version 1.7.7.[12] The structural models for mullite, cristobalite and corundum used in the analysis were based on the crystal values reported in references.[13–15] The parameters that were refined during the analysis included the scale factors for the various crystalline phases, the cell dimensions, the atomic coordinates, the occupancies and the anisotropic temperature factors, as well as the peak shape of the main phase, mullite. Since cristobalite and corundum occurred as minor phases in the treated surface layers, their peaks in the XRD spectra were very weak. Thus, the lattice parameters for cristobalite and corundum were not refined during the analysis.

The refinements for the atomic occupancies of mullite were carried out from consideration of the variations in the occupancies of the T*(Al) and O*(O) positions, associated with occupancies of the T(Si) and O_C(O) positions, under constraint of the valence equilibrium between the cations and oxygen anions, according to the following reaction:[9]

$$2Si^{4+} + O^{2-} = 2Al^{3+} + V_{\ddot{O}} \quad (2)$$

For the case of Cr atoms incorporated into mullite, these atoms replaced a fraction of the Al atoms at the 2a site.[16] The occupancies of both the Cr and Al atoms at this site were refined, under the constraint of their sum being equal to a full occupancy value of 1.

It was possible that the seven trace elements, P, Ti, Fe, Mg, Na, K and Ca in the as-received refractory brick, occupied a few sites of the Al and Si atoms of mullite crystals after the laser melting. On the one hand, it was very difficult to model so many atoms in the crystalline structure. On the other hand, the effects of these trace atoms on the refinements were negligible provided that good fittings between the observed and calculated spectra can be achieved as shown below. Thus, the occupancies of these trace atoms were not taken into account during the analysis.

The peak shape was described using a pseudo-Voigt distribution with the Howard asymmetry, and the background was described by an automatic smoothed curve to exclude the broadened halo of the amorphous phase, with 2θ values from 17 to 26°.[12]

In addition, polished cross sections of the treated surface layers were observed using an AMRAY 1810 scanning electron microscope (SEM) to observe the basic microstructural features. For preparation of polished cross sections, the samples were first cut to the required dimensions, 28×10×5 mm, and then mounted in epoxy resin. The mounted samples were successively ground with Struers MD-Piano 220 and MD-Allegro (with diamond slurry, 15 μm in size) for 5 and 10 min and, finally, polished using MD-Plan and MD-Dac clothes with diamond slurries of 6 and 3 μm for 15 and 60 min, respectively.

3. Results and discussion

3.1. Microstructural characterization

SEM observations indicated that the flame sprayed coatings, FAA and FCA, still retained the lamellar structure and mechanical bonding to the substrate, typical of thermal sprayed coatings,[17] despite the fact that a very slow workpiece traverse velocity of 4 mm/s was used in the present work. The amount of flattening of the Cr_2O_3 lamellae was greater than that of the Al_2O_3 lamellae in the coating, FCA [Fig. 3(a) and (b)].

The microstructures of the samples, LFAA and LF00, were similar to that of sample L000 [Fig. 3(c) and (d)]. The surface layers mainly consisted of elongated crystals in a matrix consisting of eutectic mixture, in addition to some pores and cracks. Although some microstructural differences were observed, more than 75% of the as-treated surfaces consisted of the elongated crystals, with elongated axes approximately perpendicular to the surface. These elongated crystals have a whisker-like morphology, but their diameters, 10–20 μm are relatively large.[5]

The morphology of the elongated crystals in sample LFCA was also similar to those for samples LFAA, LF00 and L000. However, the elongated axes of the crystals in sample LFCA appeared to be predominantly parallel to the as-treated surface. Consequently, the as-treated surface was pore-free and there were fewer cracks within the surface layer [Fig. 3(e) and (f)].

3.2. Phase constituents and crystalline orientation

From the XRD spectra collected from the as-treated surfaces of the various samples (Fig. 4), it can be seen that the flame sprayed coating, FAA, mainly consisted of α-Al_2O_3 with a small amount of β-Al_2O_3. When 20% Cr_2O_3 by weight was added to the Al_2O_3 powder, the resulting flame sprayed coating, FCA, contained some metastable γ-Al_2O_3, in addition to corundum (α-Al_2O_3), β-Al_2O_3 and eskolaite. The amount of eskolaite in the coating, FCA, was slightly greater than that of the starting 20%Cr_2O_3–80%Al_2O_3 powder (Fig. 1).

The broadened halos, for 2θ values from 17 to 26°, apparent in the XRD spectra, suggested that there was

some amorphous phase in the surface layers of samples: L000 and LF00. Since these broadened halos had centres at the (101) reflection for cristobalite, the amorphous phase in the two samples was probably SiO_2. From the relative integrated intensities of the two broadened halos, it can be concluded that flame preheating decreased the amount of amorphous SiO_2 in the laser-treated surface layer. There was no appreciable amorphous phase in the surface layers of the combined flame- and laser-treated samples LFAA and LFCA.

Despite the absence of some diffraction peaks for mullite, the main phase in the as-treated surfaces of the four samples: L000, LF00, LFAA and LFCA, prepared using laser melting and the combined flame and laser treatment, was identified as mullite (Fig. 4). This is because the various preferred orientations of the elongated grains have been observed in the SEM [Fig. 4(d) and (f)], and the XRD spectra collected from crushed and milled particles confirmed that the four treated surface layers mainly consisted of mullite (Fig. 5). In Fig. 5, the relative intensities of the amorphous SiO_2 halos for samples L000 and LF00 were somewhat less than those in Fig. 4. This may be due to the fact that the cooling and solidifying rates around the melt surfaces were higher, resulting in greater amounts of amorphous phase in the outer regions than in the internal regions of the treated surface layers. The absence of some peaks for mullite in the XRD spectra of the as-treated surfaces was associated with the crystalline orientations of the mullite crystals. For samples L000, LF00 and LFAA, the preferred orientation was along the [111] direction. Consequently, the peaks for (220) and (130) were

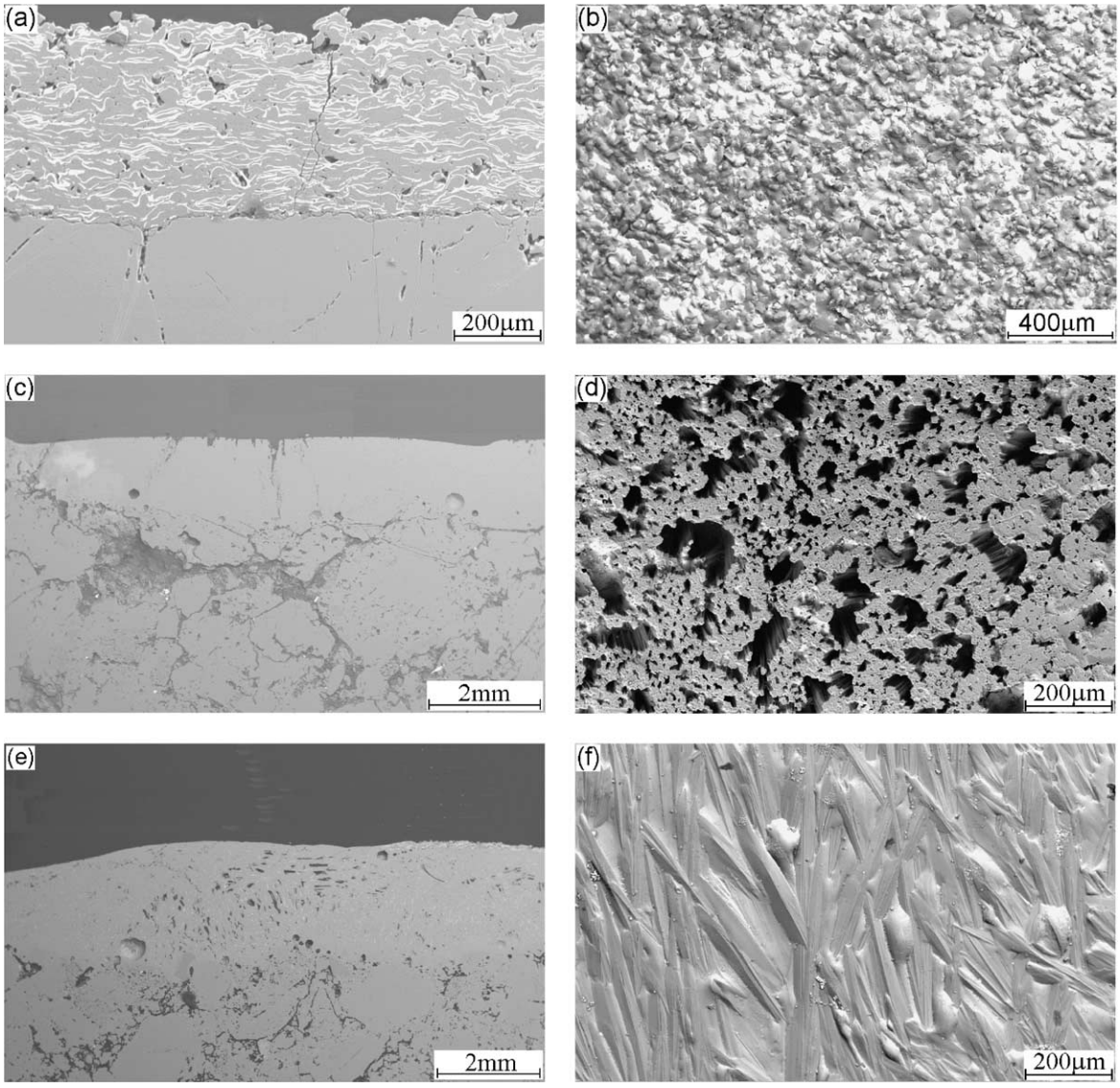

Fig. 3. Scanning electron microscopy images of samples (a) FCA, polished cross section, (b) FCA, as-sprayed surface, (c) L000, polished cross section, (d) L000, as-treated surface, elongated axis of the crystals approximately perpendicular to the surface and many surface pores, (e) LFCA, polished cross section, (f) LFCA, as-treated surface, elongated axis of the crystals approximately parallel to the pore-free surface.

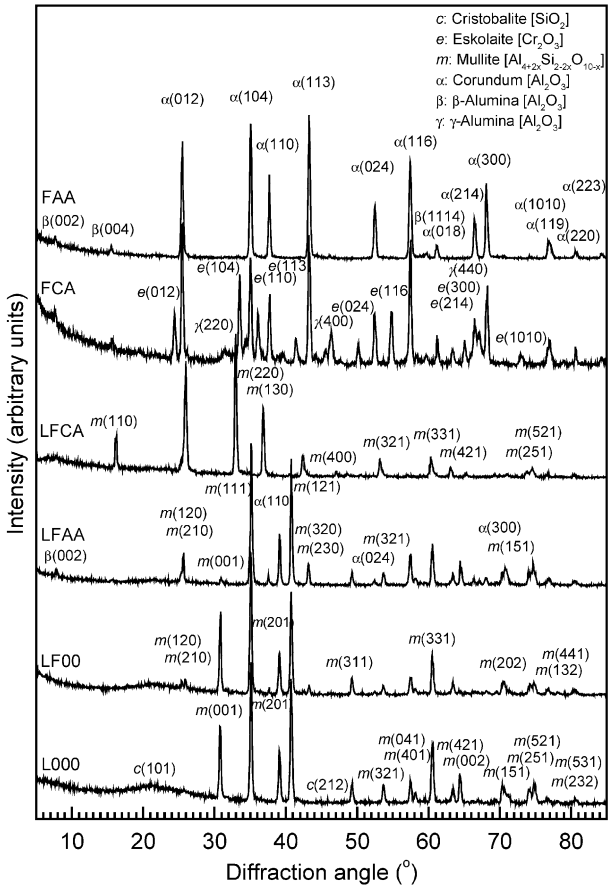

Fig. 4. XRD spectra collected from the as-treated surfaces of the various samples, identifying their phase constituents and crystalline orientations.

absent, and the pair peaks for (120) and (210) were very weak. For sample LFCA, the preferred orientation was along the [220] direction, and the peaks for (111), (201), (121) and (321) disappeared (Fig. 4).

3.3. Lattice parameters for mullite crystals

The formation conditions for the crystals varied across the melt pools during the laser and the combined flame and laser processing;[3] the lattice parameters for the refined mullite crystals should be taken as the "average" values within the corresponding surface layers. During the X-ray Rietveld analysis, automatic smoothed backgrounds were used to exclude the amorphous broadened halos in the XRD spectra for samples: L000 and LF00. Good fittings between the observed and calculated intensities have been achieved for the as-received refractory ceramic and the four treated surface layers. Fig. 6 shows the X-ray Rietveld refinement plot for the sample L000. Table 2 lists the refined parameters and contents of the crystalline phases for the as-received refractory ceramic and the four treated surface layers. The reliability factors for the present refinements listed in Table 2 were larger than those for mullite structures using synchrotron radiation XRD data,[9] but lower than those for $(Cr_xV_{1-x})_2O_3$ structures using standard XRD data.[18]

The mullite in the as-received refractory ceramic had the lowest value of x, 0.22, indicating the largest amount of incorporated SiO_2. Correspondingly, the cell parameters, a and c, were also the smallest of all the

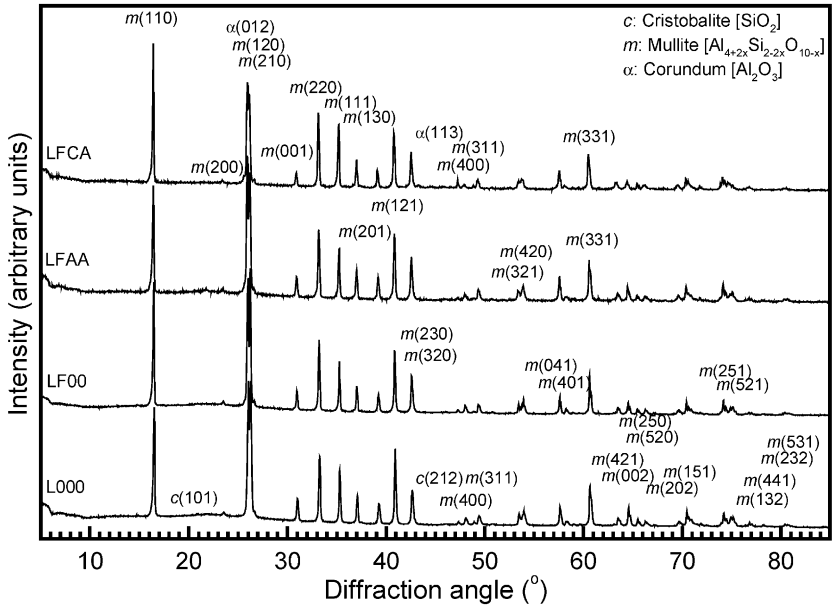

Fig. 5. XRD spectra collected from the milled particles of the four surface layers prepared using laser treatment and the combined flame spraying and laser treatment process, showing that the main phase is mullite.

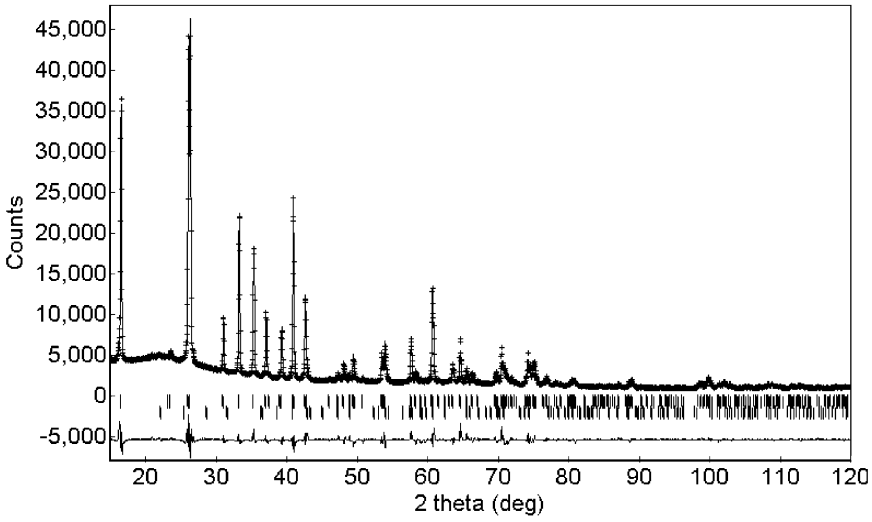

Fig. 6. X-ray Rietveld refinement plot for sample L000C. The upper solid line is the best-fit profile, and the points superimposed on it are the raw data. The upper row of tick marks indicates the position of the Bragg reflections for mullite, and the lower for cristobalite. The lower curve indicates the difference between the observed and calculated patterns.

samples. The as-received brick contained about 5% cristobalite by weight, in addition to mullite.

After laser surface melting, the amount of SiO_2 incorporated in the mullite crystals of sample L000 obviously decreased. Consequently, the cell parameters, *a* and *c*, increased to some extent, while the cell parameter, *b*, decreased slightly. The amount of crystalline cristobalite clearly decreased.

Preheating using a flame without any powder feedstock resulted in a further decrease in the amount of SiO_2 incorporated in the mullite crystals of sample LF00, and increases in the cell parameters: *a*, *b* and *c*. The amount of crystalline cristobalite also further decreased when compared with that in the laser-treated sample, L000.

When pure Al_2O_3 powder was used as the feedstock for flame spraying in the combined process, the amount of SiO_2 incorporated in the mullite crystals decreased slightly, and the cell parameters: *a*, *b* and *c* increased slightly in the treated surface layer LFAA when compared with those for the surface layer, LF00 produced using the combined process without any powder feedstock for flame spraying. However, the amount of crystalline cristobalite in LFAA was somewhat increased compared with that in LF00.

For the sample, LFCA, prepared using a composite powder of 20% Cr_2O_3 and 80% Al_2O_3 by weight as the feedstock for flame spraying in the combined process, the amount of SiO_2 incorporated in the mullite crystals clearly increased when compared with that for sample LFAA produced using pure Al_2O_3 as feedstock in the combined process. The amount of SiO_2 incorporated in the mullite crystals of this surface layer was closer to that in stoichiometric mullite, with a value for *x* equal to 0.25.[5] Due to Cr for Al substitution, the cell parameters, *a* and *c*, for mullite in this sample were larger than those in sample LFAA despite a lower amount of SiO_2 incorporated in the mullite.

4. Discussion

While the predominant phase in plasma sprayed alumina coatings on metallic substrates is the metastable γ-Al_2O_3,[19,20] the predominant phase in the present flame sprayed Al_2O_3 and 20%Cr_2O_3–80%Al_2O_3 coatings was stable α-Al_2O_3. This may be is due to a greater number of partially molten Al_2O_3 particles being embedded in the flame sprayed coatings than in the plasma sprayed coatings. The presence of partially molten Al_2O_3 particles embedded in the sprayed coatings has been confirmed by the presence of some β-Al_2O_3 in the coatings.[21] On the other hand, it may be attributed to the low thermal conductivity of the refractory substrate and the very slow workpiece traverse velocity of 4 mm/s employed in the present work, resulting in the cooling and solidifying rates of the molten alumina during the spraying being much lower than those attained during plasma spraying. Plasma spraying generally uses workpiece traverse velocities of several hundreds of mm/s.

The sequence of alumina phases formed from molten alumina during the spraying process was $\gamma \rightarrow \delta \rightarrow \theta \rightarrow \alpha$.[21] Although separate Cr_2O_3 and Al_2O_3 lamellae were observed from the SEM micrographs [Fig. 3(a)], some

intermixing of Cr_2O_3 and Al_2O_3 occurred when they contacted each other in molten state. Some metastable γ-Al_2O_3 was present in the flame sprayed 20%Cr_2O_3–80%Al_2O_3 coating, but not in the pure Al_2O_3 coating (Fig. 4). This is probably attributed to larger the Cr ionic size that retarded the transition to the α-Al_2O_3 phase.[22]

The amount of eskolaite in the FCA coating was greater than that in the starting powder. This may be ascribed to more effective melting of the Cr_2O_3 particles than the Al_2O_3 particles during flame spraying, because Cr_2O_3 has a higher thermal conductivity than Al_2O_3.[23] This was also confirmed by greater flattening of the

Table 2
Refined parameters of the as-received refractory brick and the four treated surface layers

Sample code	As-received brick	L000	LF00	LFAA	LFCA	
Reliability factor	R_P	0.08	0.044	0.045	0.057	0.070
	R_{WP}	0.12	0.066	0.066	0.079	0.099
	R_{exp}	0.38	0.028	0.033	0.044	0.045
Mullite $[Al_{4+2x}Si_{2-2x}O_{10-x}]$	a (nm)	0.75352(3)	0.75687(2)	0.75737(2)	0.75756(3)	0.75966(3)
	b (nm)	0.76833(2)	0.76819(2)	0.76865(2)	0.76906(3)	0.768989(8)
	c (nm)	0.28825(1)	0.288376(8)	0.288579(7)	0.28877(1)	0.28926(1)
	V (nm^3)	0.16689	0.16825	0.16800	0.16824	0.16898
	Density (g/cm^3)	3.183	3.161	3.145	3.137	3.296
	X(1)	0.0	0.0	0.0	0.0	0.0
	Y(1)	0.0	0.0	0.0	0.0	0.0
	Z(1)	0.0	0.0	0.0	0.0	0.0
	B(1)	3.1(1)	3.96(8)	3.74(8)	3.02(9)	5.2(2)
	Occ.(1), Al	1.0	1.0	1.0	1.0	0.76(2)
	Occ.(1), Cr					0.24(2)
	X(T)	0.1509(5)	0.1536(3)	0.1507(4)	0.1539(4)	0.1553(6)
	Y(T)	0.3414(5)	0.3417(4)	0.3424(4)	0.3422(5)	0.3392(6)
	Z(T)	0.5	0.5	0.5	0.5	0.5
	B(T)	3.7(1)	4.44(8)	4.17(9)	3.6(1)	4.0(1)
	Occ.(T), Al	0.5	0.5	0.5	0.5	0.5
	Occ.(T), Si	0.387(5)	0.370(3)	0.340(5)	0.331(5)	0.358(6)
	X(T*)	0.283(3)	0.279(2)	0.282(2)	0.276(2)	0.290(2)
	Y(T*)	0.220(3)	0.220(2)	0.226(2)	0.229(2)	0.210(2)
	Z(T*)	0.5	0.5	0.5	0.5	0.5
	B(T*)	1.5(7)	1.0(4)	4.8(6)	4.5(6)	−1.6(4)
	Occ.(T*), Al	0.112(5)	0.130(3)	0.160(5)	0.169(5)	0.142(6)
	$X(O_{ab})$	0.3519(7)	0.3563(6)	0.3560(6)	0.3538(7)	0.352(1)
	$Y(O_{ab})$	0.4290(7)	0.4218(4)	0.4239(4)	0.4212(5)	0.4189(7)
	$Z(O_{ab})$	0.5	0.5	0.5	0.5	0.5
	$B(O_{ab})$	4.4(2)	4.0(1)	4.1(1)	3.6(1)	3.5(2)
	$Occ.(O_{ab})$	1.0	1.0	1.0	1.0	1.0
	$X(O_d)$	0.1270(6)	0.1300(5)	0.1295(5)	0.1292(6)	0.1405(8)
	$Y(O_d)$	0.2340(6)	0.2233(4)	0.2257(5)	0.2298(6)	0.2290(7)
	$Z(O_d)$	0.0	0.0	0.0	0.0	0.0
	$B(O_d)$	4.4(2)	4.9(1)	5.3(1)	5.0(1)	4.6(2)
	$Occ.(O_d)$	1.0	1.0	1.0	1.0	1.0
	$X(O_c)$	0.5	0.5	0.5	0.5	0.5
	$Y(O_c)$	0.0	0.0	0.0	0.0	0.0
	$Z(O_c)$	0.5	0.5	0.5	0.5	0.5
	$B(O_c)$	5.5(4)	4.5(3)	2.8(3)	1.5(4)	1.8(4)
	$Occ.(O_c)$	0.66(2)	0.61(1)	0.52(1)	0.49(2)	0.65(2)
	$X(O_{c*})$	0.453(8)	0.423(4)	0.420(4)	0.424(4)	0.418(7)
	$Y(O_{c*})$	0.124(8)	0.120(5)	0.079(4)	0.096(5)	0.075(6)
	$Z(O_{c*})$	0.5	0.5	0.5	0.5	0.5
	$B(O_{c*})$	4.4(2)	4.0(1)	4.1(1)	3.6(1)	3.5(2)
	$Occ.(O_{c*})$	0.112(5)	0.130(3)	0.160(5)	0.169(5)	0.142(6)
	Mullite x	0.22(1)	0.260(6)	0.320(9)	0.34(1)	0.28(1)
	wt.%	94.79(1.83)	99.83(1.34)	99.96(1.48)	98.75(1.71)	97.83(2.83)
Cristobalite [SiO_2]	wt.%	5.21(0.17)	0.17(0.08)	0.04(0.03)	1.25(0.20)	
Corundum [$(Al,Cr)_2O_3$]	wt.%					2.17(0.23)

Cr_2O_3 lamellae than the Al_2O_3 lamellae in the coating, FCA [Fig. 3(a) and (b)].

The presence of amorphous SiO_2 in the laser-treated surface layer, L000, was due to rapid cooling and solidification of the melt pool during processing. Flame preheating resulted in a decrease in the total amount of SiO_2, including amorphous SiO_2, crystalline cristobalite and that incorporated in the mullite crystals, in the treated surface layer, LF00. This suggests that, on the one hand, flame preheating led to relatively lower cooling and solidification rates for the melt pool. On the other hand, evaporation of SiO_2 occurred during processing. If evaporation of SiO_2 also occurred during laser melting, it may be concluded that more SiO_2 would have evaporated when the flame preheating was used.

Very little amorphous phase was observed for the surface layers prepared using the combined process. This may be associated with changes in the composition of the melt pool, resulting from flame spraying using a powder feedstock. From the thicknesses of the flame sprayed coatings and the combined flame- and laser-treated layers (Fig. 3), it can be seen that 20–25% of the materials in the combined flame- and laser-treated layers came from the powder feedstocks used in the flame spaying process. This led to a greater amount of Al_2O_3 in the melt pools formed by the combined process than by the single laser process or by the combined process without use of a powder feedstock. It is interesting that the two types of powders resulted in different amounts of SiO_2 being incorporated in the mullite crystals. Consequently, smaller amounts of cristobalite and corundum were present in the two surface layers.

It is also interesting that the use of 20%Cr_2O_3–80%Al_2O_3 by weight of composite powder resulted in change in the crystalline orientation of the mullite crystals in the surface layer prepared using the combined process. The variations in the crystalline orientations of the mullite crystals in the various laser-treated and the combined flame- and laser-treated surface layers were in good agreement with the variations in the preferred orientations of the elongated axes of the crystals [Fig. 3(d) and (f)]. Elongated crystals generally grow along the directions of heat release.[24] In the present case, the directions of maximum heat release of the molten surface during cooling and solidification probably corresponded to the melt flow directions. Thus, the changed crystalline orientation of the mullite crystals may be ascribed to a modification in the flow characteristics of the molten surface caused by the addition of Cr_2O_3.

Because of the different formation conditions, it is difficult to compare the cell parameters of the present mullite crystals with those reported in the literature.[8,9,13–16,25] In fact, the structure of mullite is still not well understood. The cell parameters, a and c, of the present mullite crystals and their variations with values of x for the as-received refractory ceramic and the samples, L000, LF00 and LFAA, are in good agreement with those reported previously.[25] It is also reasonable that the cell parameters, a, b, c, of the mullite in sample, LFCA, are between those of the mullite with an identical value of x and Cr-mullite because the amount of Cr_2O_3 incorporated in the mullite of sample LFCA was lower than that in Cr-mullite.[16] However, there is an anomaly for the variation in cell parameter, b, with the value of x for the as-received refractory ceramic and the samples: L000, LF00 and LFAA. Previously, it was reported that the value of b remains approximately constant or decreases slightly with increasing value of x.[25] Presently, there is a trend that b increases slightly with increasing value of x, despite the fact that the differences between the present b values and previous b values are rather small. For approximately identical amounts of SiO_2 incorporated in mullite crystals, the present cell parameters, a and c, for mullite crystals are larger than those for the mullite crystals developed from devitrification of quenched mullite.[9]

It is known that the mullite crystals formed from melt generally have the values of x about 0.4.[9] In the present samples, the mullite crystals produced from solidification of laser-induced melt pools all had the values of x clearly lower than 0.4. Such a result can reasonably be attributed to the solid-state chemical reactions that occurred during the processing. This is due to the fact that following the formation of the high-alumina mullite crystals from melts, solid state chemical reactions between the solid high-alumina mullite crystals and the viscous SiO_2-rich fluids probably took place before the completion of cooling and solidification, resulting in reducing the values of x of the final mullite crystals. Also, the addition of Cr_2O_3 probably promoted the flow of the viscous fluid and the solid state chemical reaction; thereby, the amount of SiO_2 incorporated in the mullite crystals of the sample LFCA appeared higher than that of the sample LFAA. As for a few amount of corundum existing in sample LFCA, this may be related to the relatively higher deposition efficiency of the 20 wt.%Cr_2O_3–80 wt.%Al_2O_3 composite powder than that of the pure Al_2O_3 powder during the spraying. Consequently, local laser-induced melt was extremely alumina-rich and a little corundum was formed during the solidification of such alumina-rich melt.

5. Conclusion

The predominant phase in flame sprayed Al_2O_3 and 20%Cr_2O_3–80%Al_2O_3 coatings was stable α-Al_2O_3. In addition of 20% Cr_2O_3 by weight to the Al_2O_3 powder retarded the phase transition of metastable γ-Al_2O_3 to α-Al_2O_3 during flame spraying.

There were certain amounts of the amorphous SiO_2 phase in the laser-treated surface layers. Flame pre-

heating decreased the amount of amorphous SiO_2 phase in the layer. There was no appreciable amorphous phase in the surface layers prepared using the combined flame spraying and laser treatment.

The mullite crystals preferred to grow along the [111] direction for the surface layers prepared by laser melting and by the combined process in which pure Al_2O_3 powder was used as the feedstock for flame spraying. In the latter case, the surface layer contained more alumina-rich mullite and more crystalline cristobalite than the laser treated surface layers. The cell parameters, a and c, of the mullite crystals and their variations with value of x for the as-received refractory ceramic and the treated surface layers were in good agreement with those reported in previous literature. There was a slight anomaly for the variation in cell parameter, b, with value of x.

When 20% Cr_2O_3 and 80% Al_2O_3 by weight composite powder was used as the feedstock in the combined process, not only was the preferred orientation of the mullite grains changed to be along the [220] direction, but also the amount of SiO_2 incorporated in the mullite crystals was closer to that for stoichiometric mullite. The values for cell parameters: a, b, c of the mullite in the treated surface layer were between those of the mullite with an identical value of x and Cr-mullite.

Acknowledgements

This research was funded by the Engineering and Physical Science Research Council (Grant Ref. GR/N08124) in collaboration with Cleanaway Ltd, BNFL, Morgan Materials Technology Ltd, ICI and Plasma Thermal Coatings Ltd. The authors are also grateful to Mr. D. Moore of the UMIST Corrosion and Protection Centre and Ms. J. Shackleton of the UMIST Materials Science Centre for their help with SEM examinations and XRD analysis, respectively.

References

1. Li, J. F., Li, L. and Stott, F. H., Statistical approach for minimizing cracks in combined flame spraying and laser surface modification of refractory ceramics. *J. Eur. Ceram. Soc.* (submitted for publication).
2. Li, J. F., Li, L. and Stott, F. H. Surface modification of refractory ceramics using combined flame spraying and laser surface coating. Accept by ICALEO 2003, *22nd International Congress on Application of Lasers & Electro-Optics*, 13–16 October, 2003, Jacksonville, Florida, USA. 2003.
3. Bradley, L., Li, L. and Stott, F. H., Flame-assisted laser surface treatment of refractory materials for crack-free densification. *Mat. Sci. Eng.*, 2000, **A278**, 204–212.
4. Triantafyllidis, D., Li, L. and Stott, F. H., Surface treatment of alumina-based ceramics using combined laser sources. *Appl. Surface Sci.*, 2002, **186**, 140–144.
5. Lee, W. E. and Rainforth, W. M., *Ceramic Microstructures: Property Control by Processing*. Chapman & Hall, London, UK, 1994.
6. Kriven, W. M., Palko, J. W., Sinogeikin, S., Bass, J. D., Sayir, A., Brunauer, G., Boysen, H., Frey, F. and Schneider, J., High temperature single crystal properties of mullite. *J. Eur. Ceram. Soc.*, 1999, **19**, 2529–2541.
7. Shin, H., Kim, C.-S. and Chang, S., N, Mullitization from a multicomponent oxide system in the temperature range 1200°–1500 °C. *J. Am. Ceram. Soc.*, 2000, **83**, 1237–1240.
8. Ronchetti, S., Piana, M., Delmastro, A., Salis, M. and Mazza, D., Synthesis and characterization of Fe and P substituted 3:2 mullite. *J. Eur. Ceram. Soc.*, 1999, **21**, 2509–2514.
9. Johnson, B. R., Kriven, W. M. and Schneider, J., Crystal structure development during devitrification of quenched mullite. *J. Eur. Ceram. Soc.*, 2001, **21**, 2541–2562.
10. Weber, J. K. R., Cho, B., Hixson, A. D., Abadie, J. G., Nordine, P. C., Kriven, W. M., Johnson, B. R. and Zhu, D., Growth and crystallization of YAG- and mullite-composition glass fibers. *J. Eur. Ceram. Soc.*, 1999, **19**, 2543–2550.
11. Lambert, P., Marple, B. and Arsenault, B., Laser surface modification of alumina-based ceramics. In *H. In Proc. Int. Symp. On Developments Mostaghaci New Metal Alloys Appl. of Ceramics*, ed. R. A. L. Drew. Canadian Inst. Min. Metall. Pet., Montreal, Canada, 1993, pp. 515–525.
12. Hunter, B. A. and Howard, C. J. *A Computer Program for Rietveld Analysis of X-ray and Neutron Powder Diffraction Patterns.* Lucas Heights Research Laboratories of Australian Nuclear Science and Technology Organization, anonymous ftp site: ftp.ansto.gov.au/pub/physics/neutron/rietveld.
13. Balzar, D. and Ledbetter, H., Crystal structure and compressibility of 3:2 mullite. *Am. Mineralogist*, 1993, **78**, 1192–1196.
14. Dollase, W. A., Reinvestigation of the structure of low Cristobalite. *Zeitschrift fuer Kristallographie, Kristallgeometrie*, 1965, **121**, 369–377.
15. Oetzel, M. and Heger, G., Laboratory X-ray powder diffraction: a comparison of different geometries with special attention to the usage of the Cu Kα. *J. Appl. Crystallography*, 1999, **32**, 799–807.
16. Fischer, R. X. and Schneider, H., Crystal structure of Cr-mullite. *Am. Mineralogist*, 2000, **85**, 1175–1179.
17. Smith, R. W. and Novak, R., Advances and applications in U.S. thermal spray Technology: I. technology and materials. *Powder Metallurgy Int.*, 1991, **23**(3), 147–155.
18. Oyama, T., Iimura, Y. and Takeuchi, K., Synthesis of $(Cr_xV_{1-x})_2O_3$ fine particles by a laser-induced vapor-phase reaction and their crystal structure. *J. Mat. Sci.*, 1999, **34**, 439–444.
19. Krishnan, R., Dash, S., Rao, C. B., Rao, R. V. S., Tyagi, A. K. and Raj, B., Laser induced structural and microstructural transformations of plasma sprayed Al_2O_3 coatings. *Scripta Mat.*, 2001, **45**, 693–700.
20. Guilemany, J. M., Nutting, J. and Dougan, M. J., A transmission electron microscopy study of the microstructures present in alumina coatings produced by plasma spraying. *J. Thermal Spray Techn.*, 1997, **64**, 425–429.
21. Li, J. F., Li, L. and Stott, F. H., Combined Laser and Flame Surface Coating of Refractory Ceramics-phase and Microstructre Characteristics. Presented to EMRS 2003 meeting.
22. Okada, K., Hattori, A., Kameshima, Y. and Yasumori, A., Effect of monovalent cation additives on the γ-Al_2O_3 to α-Al_2O_3 phase transition. *J. Am. Ceram. Soc.*, 2000, **83**, 1233–1236.
23. Ding, C. X., Huang, B. T. and Lin, H. L., Plasma-sprayed wear-resistant ceramic and cermet coating materials. *Thin Solid Films*, 1984, **118**, 485–493.
24. Bianchi, L., Denoirjean, A., Blein, F. and Fauchais, P., Microstructural investigation of plasma-sprayed ceramic splats. *Thin Solid Films*, 1997, **299**, 125–135.
25. Cameron, W. E., Composition and cell dimensions of mullite. *Bull. Am. Ceram. Soc.*, 1977, **56**, 1003–1011.